

***Electron Microscopy  
Characterization of Tc-  
Bearing Metallic Waste  
Forms –Final Report  
FY10***

Fuel Cycle Research & Development

***Prepared for  
U.S. Department of Energy  
Separations/Waste Form Campaign  
E. C. Buck, D. Neiner  
Pacific Northwest National Laboratory  
September, 2010  
FCR&D-PN1015030307  
PNNL-19837***



**DISCLAIMER**

This information was prepared as an account of work sponsored by an agency of the U.S. Government. Neither the U.S. Government nor any agency thereof, nor any of their employees, makes any warranty, expressed or implied, or assumes any legal liability or responsibility for the accuracy, completeness, or usefulness, of any information, apparatus, product, or process disclosed, or represents that its use would not infringe privately owned rights. References herein to any specific commercial product, process, or service by trade name, trade mark, manufacturer, or otherwise, does not necessarily constitute or imply its endorsement, recommendation, or favoring by the U.S. Government or any agency thereof. The views and opinions of authors expressed herein do not necessarily state or reflect those of the U.S. Government or any agency thereof.

## SUMMARY

The DOE Fuel Cycle Research & Development (FCR&D) Program is developing aqueous and electrochemical approaches to the processing of used nuclear fuel that will generate technetium-bearing waste streams. This report presents Pacific Northwest National Laboratory (PNNL) research in FY10 to evaluate a Fe-based alloy waste form for Tc that provides high waste loading within waste form processing limitations displays long-term retention of radionuclides and can be produced with consistent physical, chemical, and radiological properties for eventual disposal.

Fe-Mo metallic waste forms are being considered for the retention and ultimate long-term disposal of Tc from used nuclear fuel recycle. We have conducted microanalysis with scanning electron microscopy (SEM) and transmission electron microscopy (TEM) of non-radioactive FeMo-Re alloy, non-radioactive undissolved solids (UDS) alloy, and radioactive FeMo-Tc alloy samples. The concentration of Tc and Re in the alloy melt was between 2 and 11 at%. SEM analysis indicated the presence of two major phases; an Fe-rich phase and a mixed Fe-Mo alloy. The Fe-Mo phase was also present in the UDS containing specimens analyzed in this study. The TEM compositional analysis of the dominant Fe-Mo phase in the alloys indicated a ratio of 2:1 for Fe:Mo. Electron diffraction investigation of the Fe-Mo phase suggested a Laves-type C14 phase,  $\text{MoFe}_2$ . This identification was consistent with literature studies on the Fe-Mo system and the conditions of formation. Tc and Re resided principally in the intermetallic phases in the respective waste form alloys in the simpler systems. With the addition of Pd and Rh (UDS elements) into the alloy composition, Re was no longer associated with the  $\text{Fe}_2\text{Mo}$  intermetallic. Because of the structural and compositional similarity of the intermetallics in the waste form samples, it is concluded that Re is an excellent substitute for Tc in these types of nuclear waste form materials.



## CONTENTS

1.	Introduction .....	1
2.	Experimental Procedure .....	3
3.	FeMo Characterization .....	4
4.	UDS Characterization.....	10
5.	Discussion.....	13
6.	Conclusion.....	15
7.	References .....	16

## FIGURES

Figure 1.1	Phase diagram for the Fe-Mo system (adapted from [9]).....	2
Figure 3.1	SEM analysis of FeMo-Re alloy; iron map, molybdenum map, rhenium map, and backscattered electron image.....	4
Figure 3.2	SEM analysis of FeMo-Re alloy; The RGB combination map used a mixture of elemental maps; iron, rhenium, and molybdenum. The instrument generated a map with Zr although Zr is not present in the alloy. ....	5
Figure 3.3	<b>B</b> 1210 Zone axis pattern from the (i) FeMo-Tc phase and the (ii) FeMo-Re phase. ....	6
Figure 3.4	<b>B</b> [0111] Zone axis patterns from the (i) FeMo-Tc and (ii) FeMo-Re phases. The Re-rich phase pattern has been rotated to show the patterns are slightly distorted hexagonal patterns and are identical. Both phases had the same inter-planar spacings (within measuring errors) and internal angles. ....	7
Figure 3.5	TEM Images of FeMo-Tc Alloy. (a) Showing lattice fringes (yellow arrow) and Moiré fringes (blue arrows) and (b) a grain boundary (g.b.).....	7
Figure 3.6	XRD Comparison of the (a) FeMo-Re and (b) FeMo-Tc alloys. ....	8
Figure 4.1	Shows the isolation of a region of the non-radioactive UDS alloy prepared by focused ion beam. The Rh-Pd rich regions were isolated and marked with a deposit of carbon (A), these were then ion beam etched and removed with a nano-probe (B), the specimen was then welded to milling station (C) and the ion milled (D), until electron beam transparent (E). ....	10
Figure 4.2	Showing the three main phases in the sample ( $\alpha$ -Fe, Fe <sub>2</sub> Mo, and the hexagonal Pd-Re alloy). The spectra for the iron phases have been normalized to the iron Fe-K $\alpha$ signal intensity. ....	11

Figure 4.3 Elemental Map showing the occurrence of Re and Pd in the same phase and a significantly lower level of Re in the Mo-Fe intermetallic..... 11

Figure 4.4 Line profiles through different phases in the UDS alloy ..... 12

Figure 4.5 Plot showing the distribution of elements across the Pd-rich and intermetallic regions ..... 12



## ACRONYMS

BSE	Backscattered Electron
EBR-II	Experimental Breeder Reactor-II
FCR&D	Fuel Cycle Research & Development
FIB	focused ion beam
INL	Idaho National Laboratory
PNNL	Pacific Northwest National Laboratory
SEM	Scanning electron microscopy
TEM	Transmission electron microscopy
UDS	Undissolved Solids





# Technetium Waste Form Development – Final Report

## 1. Introduction

This report is an update of the work on the Tc alloy waste form development characterization work at Pacific Northwest National Laboratory (PNNL) in fiscal year 2010. Recycling of spent or used nuclear fuel may offer some significant advantages over direct disposal into geologic repository in terms of materials recovery and volume reduction [1]. Nevertheless, the environmental issues associated with the disposal of long-lived radioisotopes, such as  $^{99}\text{Tc}$  ( $t_{1/2} = 2.13 \times 10^5$  a), is unlikely to disappear and may require the production of suitably durable nuclear waste forms. Better engineered nuclear waste forms are being considered for specific waste streams. The behavior of the advanced waste forms need to be evaluated in terms of the full range of environmental conditions that are possible within a repository setting [2]. Changes in environmental conditions are expected, and may originate from the waste forms themselves (e.g., heat, radiation damage, waste form corrosion), or may reflect the natural variability of the repository setting (e.g., water seepage rates, mechanical stability). In some cases, the environmental setting may directly reflect the durability of the waste form itself. It is important to have a good understanding of the microstructure of the waste forms to develop effective models for long-term corrosion and to build scientific basis for the disposal strategy.

Metallic waste forms have been previously developed by Idaho National Laboratory (INL) for the Experimental Breeder Reactor-II wastes [3-5]. The minimum additive waste stabilization approach is being utilized to produce a metal waste form that both addresses the performance goals and minimizes the amount of additional materials that needs to be added to make a durable material. Previous work had revealed a complex microstructure with multiple phases in the Fe-Mo-Zr system for metallic waste form alloys [6]. In this study, a 48wt% Fe, 38 wt% Mo, with 14 wt% Re alloy (termed FeMo-Re alloy in this paper) and a 52 wt% Fe, 41 wt% Mo with 7 wt% Tc (termed FeMo-Tc alloy) were prepared at INL [7]. The UDS samples contained Pd and Rh in addition to Fe, Mo, and Re. All samples were analyzed for further with electron microscopy.

The melting points for  $\alpha$ -Fe and pure Mo are 1538°C and 2623°C, respectively. The  $\lambda$ -phase is the Laves intermetallic,  $\text{MoFe}_2$ . The intermetallic ( $\lambda$ ) phase crystallizes in the  $\text{MgZn}_2$ -type hexagonal structure, designated C14. The structures of Tc-Zr alloys for waste immobilization have been reported by Poineau et al. (2009) [8]. Tc-Zr binary alloys yield a series of phases including a hexagonal  $\text{Tc}_2\text{Zr}$ . The FeMo-Tc alloy contains significantly smaller amounts of Tc than these phases and Tc (or Re in the FeMo-Re alloy) may not be a structurally critical element in any phase. The phases are dominated by the Fe-Mo system which includes FeMo and  $\text{Fe}_2\text{Mo}$  [9] (see Figure 1.1).

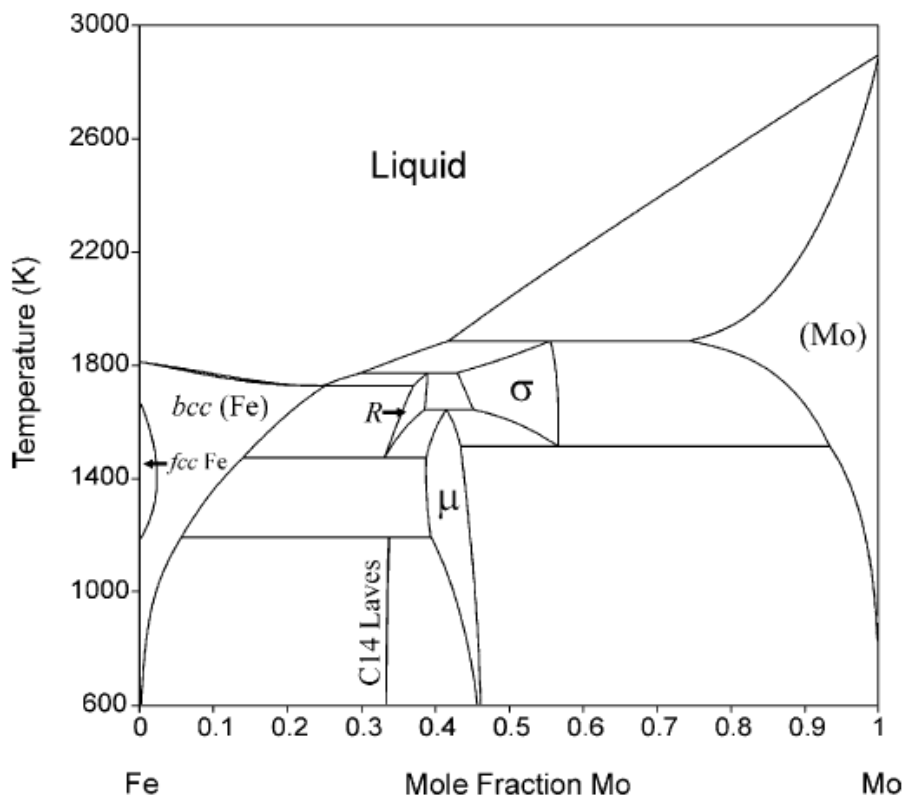


Figure 1.1 Phase diagram for the Fe-Mo system (adapted from [9])

## 2. Experimental Procedure

The ingots were prepared at INL with a defined composition of 71.3 wt% 316SS-5.3 wt% Zr-13.2 wt% Mo-4.0 wt% Ru-6.2 wt% Re [7]. For SEM, a section of the ingot was prepared as a metallographic mount and final polished on a vibratory Syntron, first with one micrometer diamond on a nylon lapping cloth and then with colloidal silica on a super fine felt cloth. For TEM, 3-mm diameter slices were diamond polish dimpled (first with 6-micron diamond paste and then with 0 to 2  $\mu\text{m}$  cubic boron nitride (CBN) and ion milled using standard Gatan procedures. The metallic waste form sample was extremely brittle and during the first TEM sample preparation attempt, the thin-foil broke during handling. A second specimen was epoxy impregnated prior to final polishing and ion milling. The UDS samples were prepared using a Dual Beam Focused Ion Beam (FIB) instrument (FEI Helios NanoLab). This is discussed in more detail in a later section.

The metallic nuclear waste form samples were analyzed with an FEI (Hillsboro, OR, USA) Quanta250 field emission gun scanning electron microscope equipped with a Oxford EDAX compositional analysis system and for TEM with a FEI Tecnai 30S-Twin transmission electron microscope with a  $\text{LaB}_6$  filament operated at 200-300 keV and equipped with a Gatan (Gatan Inc., Pleasanton, CA) ORIUS™ digital camera and an EDS system. The electron diffraction camera lengths were calibrated using a MAG\*I\*CAL silicon standard, as were the length scales. XRD was performed using a Scintag PAD V x-ray diffractometer. A sample of Zircaloy was used as a calibration check for the XRD system.

Diffraction patterns and electron micrographs were analyzed with Gatan DigitalMicrograph 1.83.842 and aided with custom scripts from Mitchell (2008) [10]. Crystal models and simulated diffraction pattern were generated using CrystalMaker® 2.2, a crystal and molecular structures program for Mac and Windows, and SingleCrystal®2.0.1, an electron diffraction simulation program distributed by CrystalMaker Software Ltd., Oxford, England (<http://www.crystallmaker.com>). JADE (Materials Data Inc., Livermore, CA, USA) software was used to analyze the XRD data.

### 3. FeMo Characterization

Initial SEM analyses indicated both materials were multi-phase alloys (see Figure 3.1 and Figure 3.2) exhibiting a eutectic structure consisting of an Fe solid solution (dark contrast in the backscattered electron (BSE) image) and an intermetallic phase (bright contrast). An undissolved Mo phase was also observed in the FeMo-Re alloy; whereas a similar phase was not found in the FeMo-Tc alloy. Elemental mapping of demonstrated that a majority of the Re was present in the intermetallic phase. The composition of the brittle intermetallic phase in both alloy samples was obtained with TEM-EDS.

The Mo rich phase was only observed in the FeMo-Re composition.

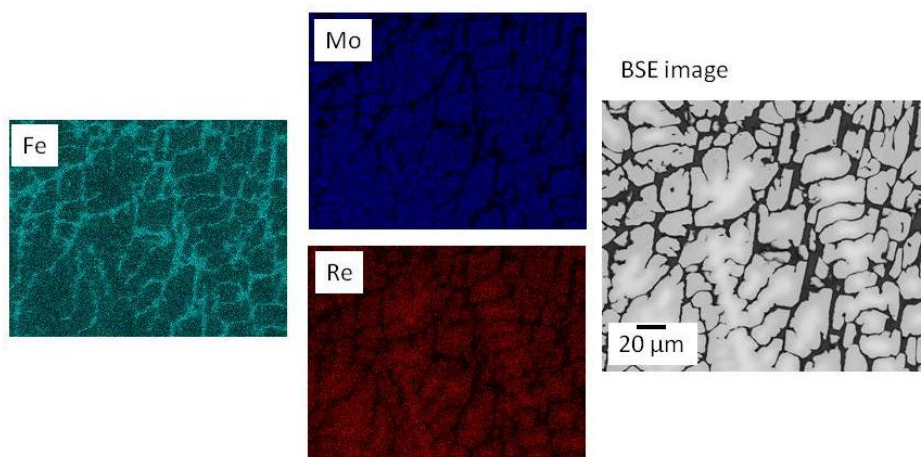


Figure 3.1 SEM analysis of FeMo-Re alloy; Fe map, Mo map, Re map, and backscattered electron image.

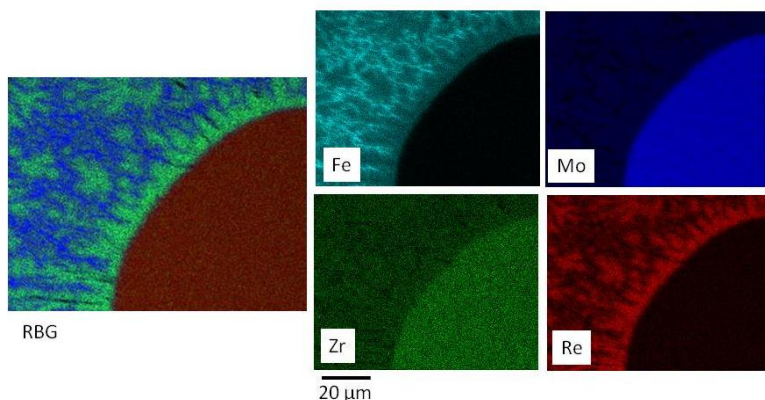


Figure 3.2 SEM analysis of FeMo-Re alloy; The RGB combination map used a mixture of elemental maps; Fe, Re, and Mo. The instrument generated a map with Zr although Zr is not present in the alloy.

Because of the strong overlap between Tc and Mo, the Mo-L line appeared more intense in the FeMo-Tc solid. The Mo-K lines at 17.37 keV were approximately same intensity in both samples because the Fe to Mo ratio was relatively constant. Re has a series of M-lines just below the Mo-L line and several L-lines at 8.651, 10.008, and 10.274 keV. The Tc-K lines are high energy lines at 18.248, 18.364, and 20.615 keV. The Mo- $L_{\alpha 1}$  (2.293 keV) and - $L_{\beta 1}$  (2.394 keV) lines from the FeMo-Tc phase were fitted using data collected from the FeMo-Re phase where there is no significant overlap problem in this energy region. To determine the possible change in X-ray peak intensity with foil thickness, the ratio of the K- to L- lines for Mo and the L- to M- lines for Re were analyzed as a function of the Fe-K to total L-line intensity. As the Fe-L intensity decreased, the foil thickness can be assumed to be increase; this has an effect on the lower energy emissions through self-absorption in the target metal. This Fe- intensity ratio was monitored during the analysis of the FeMo-Tc sample to determine if the analyses were in the same range as the ones performed with the FeMo-Re phase. The extracted compositions are listed in Table 1 for the FeMo-Re and FeMo-Tc intermetallic phases.

Table 3.1 Composition of FeMo, FeMo-Tc and FeMo-Re Phases (atomic%)

Table 3.1a. FeMo

	EDX001	EDX002	EDX003	EDX004	EDX005	EDX007		
Fe(K)	44	34	54	30	42	36		
Mo(K)	27	42	21	38	33	35		
Cr(K)	8	6	8	8	8	8		
Re(L)	14	11	8	19	9	17		
	6	3	7	3	7	4		

Table 3.1b. FeMo-Re

	EDX001	EDX002	EDX003	EDX004	EDX005	EDX007	EDX008	EDX009
Fe(K)	50	67	68	63	67	72	65	70
Mo(K)	39	26	27	31	26	20	28	24
Re(L)	11	7	6	6	7	7	7	6

Table 3.1c. FeMo-Tc

	EDX001	EDX002	EDX003					
Fe(K)	56	75	64					
Mo(K)	38	23	34					
Tc(K)	5	2	2					

Electron diffraction patterns from the two samples (FeMo-Re and FeMo-Tc) are shown in Figure 3.3 and Figure 3.4. These were taken along the same zone axis and are a strong indication of the structural similarity of the two phases. The rectangular pattern in Figure 3.3 was indexed to the  $B[1\bar{2}10]$  direction. Whereas, the partly hexagonal pattern in Figure 3.4 was indexed to the  $B[0\bar{1}11]$  direction for  $MoFe_2$ .

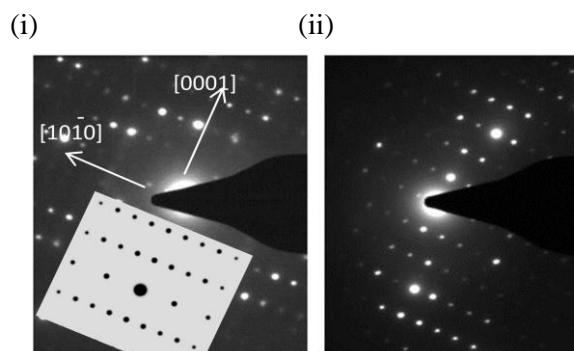


Figure 3.3  $B[1\bar{2}10]$  Zone axis pattern from the (i) FeMo-Tc phase and the (ii) FeMo-Re phase.

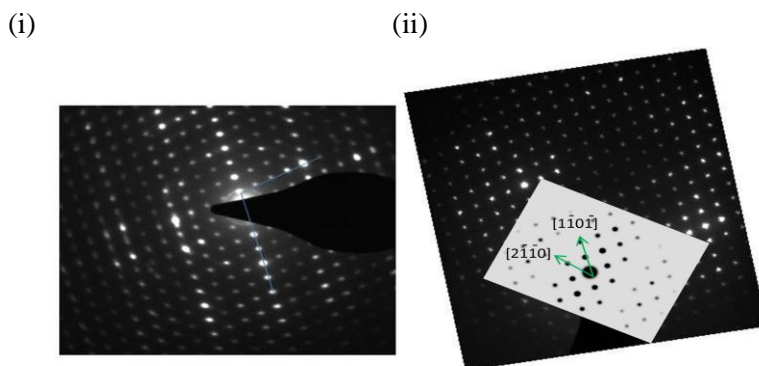


Figure 3.4  $B[0\bar{1}11]$  Zone axis patterns from the (i) FeMo-Tc and (ii) FeMo-Re phases. The Re-rich phase pattern has been rotated to show the patterns are slightly distorted hexagonal patterns and are identical. Both phases had the same inter-planar spacings (within measuring errors) and internal angles.

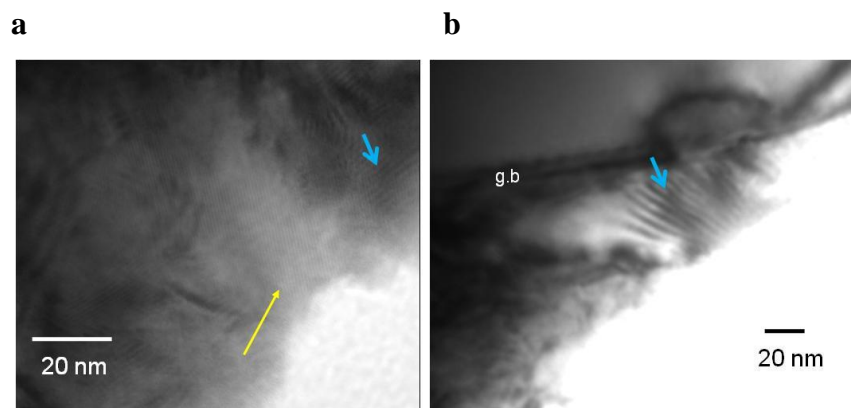


Figure 3.5 TEM Images of FeMo-Tc Alloy. (a) Showing lattice fringes (yellow arrow) and Moiré fringes (blue arrows) and (b) a grain boundary (g.b.).

The XRD patterns of the material were obtained to aid in the identification of the intermetallic phase; however, the bulk sample analyzed would have contained multiple phases from the melted specimen. The electron diffraction zone axis patterns showed a similar, if not, identical patterns. The electron diffraction patterns from the Tc sample were not as clear as the TEM photomicrographs because the specimens were a little thicker than the ones from the FeMo-Re alloy. This was due to the difficulties of handling radioactive samples. The TEM images of the

Tc-bearing phase (Figure 3.5). The EDS analyses were performed in these thin edge regions. A stacking fault consistent with the intermetallic structure is visible in the TEM images. The faint lines in the TEM images are most likely due lattice fringes from some of the large lattice spacings in these structures (marked by the yellow arrow). Other larger range contrast consistent with Moiré fringes is visible in the images (blue arrows).

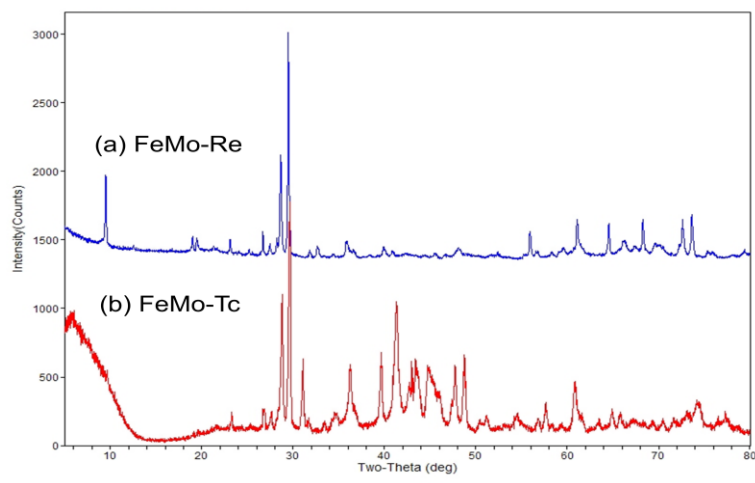


Figure 3.6 XRD Comparison of the (a) FeMo-Re and (b) FeMo-Tc alloys.

The FeMo-Re and FeMo-Tc alloys contain a dominant intermetallic phase that was structurally identical as well as compositionally similar. This phase was found in association with the  $\alpha$ -Fe (bcc) consistent with the phase diagram and in agreement with the SEM observations. The Fe content in the Fe-Mo phase was consistent with the  $\text{Fe}_2\text{Mo}$  compositional region. These phases were extremely brittle and easily separated from the iron (bcc) phase during crushing. This observation supported the identification as an ordered intermetallic phase. XRD was also performed on the intermetallic alloy to aid in the phase identification and to locate any similar phases reported in the diffraction database (see Figure 3.6). The peak fitting which is discussed later in this section resulted in a match with an orthorhombic or monoclinic phase; however, the electron diffraction data supported a phase structurally similar to hexagonal C14 Laves phase  $\text{MoFe}_2$  ( $\mathbf{a} = 4.73 \text{ \AA}$  and  $\mathbf{c} = 7.72 \text{ \AA}$ ).

The concentration of Tc and Re in the intermetallic phases ranged from 2 to 11 atomic%. In terms of waste form development this loading was expected. The Fe and Mo content was relatively stable and; generally, the Fe:Mo ratio was approximately 2:1. The major elements

were quantified using the K-lines as there was no significant overlap in this energy region and less potential self-absorption unlike the Mo-L lines.

XRD was performed on the metallic samples to aid in the analysis of the phases. This further comparison of the Fe-Mo alloys with XRD did appear to show significant differences. The analysis of the FeMo-Re phase together with a structural analysis is shown in Figure 3.6. The best fit was obtained with an orthorhombic structure; however, a reasonable fit to a monoclinic unit cell was also obtained. It is likely that other phases present in the multi-phase alloy led to the unusual result. Topological analyses of the Fe-Mo crystal structures have revealed that the  $\lambda$ -,  $\mu$ -, R-, and  $\sigma$ -phases (phases that might be present in the waste form alloy based on the phase diagram) possess exclusively tetrahedral interstices of the coordination polyhedron which allows for close-packing and leads to the relative stability of these phases [11]. This implies that monoclinic or even orthorhombic structures would be highly unfavorable. The electron diffraction pattern simulations did not match with the XRD identified phase possibilities.

The d-spacings obtained from this fit were compared with electron diffraction data from the FeMo-Tc and FeMo-Re intermetallic phases. The electron diffraction data revealed a series of large d-spacings that were not visible in the XRD results. Electron diffraction d-spacings, particularly for the large d-spacings, have a larger error ( $\pm 10\%$ ) than the corresponding XRD values. However, the large d-spacings were clearly visible on the electron diffraction patterns as strong reflections.

There was a large low angle background in the XRD scan from the FeMo-Tc sample analysis. This made comparison of the materials difficult. Indeed, there were little obvious similarities of the two materials. It should be noted that the FeMo-Re material contained an almost pure Mo phase, and that the nature of the sample preparation for XRD and the problems associated with handling Tc metal specimens may have resulted in other differences between the two materials.

## 4. UDS Characterization

The UDS samples were prepared by Dual Beam FIB etching.

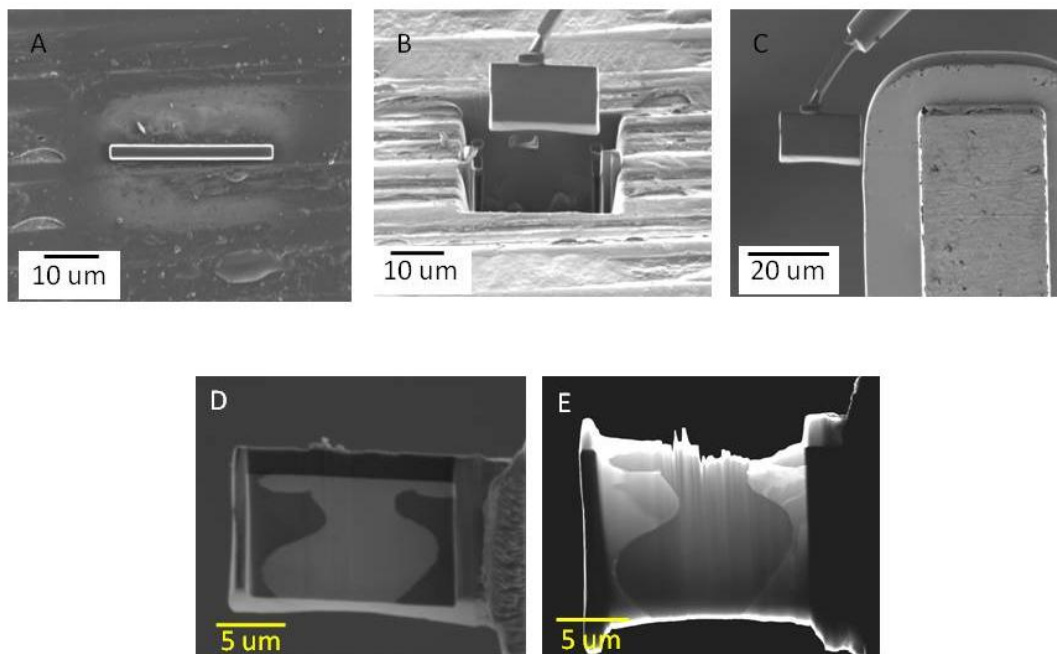


Figure 4.1 Shows the isolation of a region of the non-radioactive UDS alloy prepared by focused ion beam. The Rh-Pd rich regions were isolated and marked with a deposit of carbon (A), these were then ion beam etched and removed with a nano-probe (B), the specimen was welded to milling station (C) and the ion milled (D), until electron beam transparent (E).

The FIB prepared sample of the UDS alloy described previously was thinned to electron transparency with a 1 keV Ar ion beam. However, instead of thinning the material tended to erode at the edge with little overall thinning to improve the quality of the sample (see Figure 4.1). The sample was attached to a copper grid and then analyzed. Three phases were found in the sample. An Fe phase, the intermetallic  $\text{Fe}_2\text{Mo}$ , and the Pd-Re phase (see Figure 4.2). In the presence of the UDS material, all Re appeared to be incorporated into the Pd-rich phase rather than the intermetallic. Observation with TEM revealed a relatively plain microstructure with no obvious features.

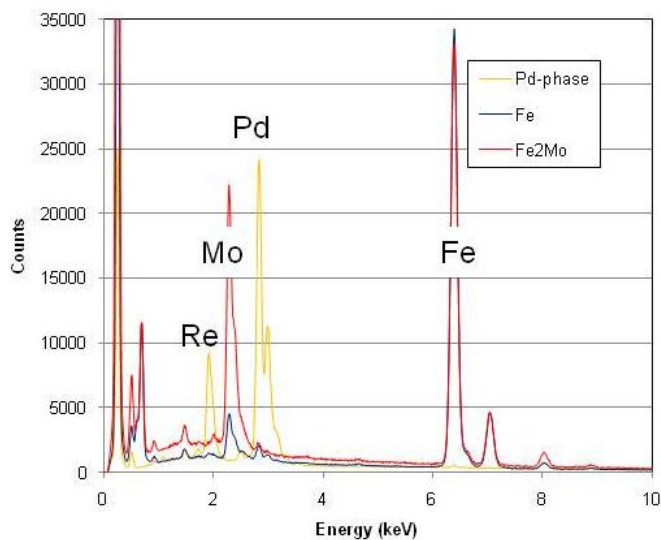


Figure 4.2 Showing the three main phases in the sample ( $\alpha$ -Fe, Fe<sub>2</sub>Mo, and the hexagonal Pd-Re alloy). The spectra for the Fe phases have been normalized to the Fe-K $\alpha$  signal intensity.

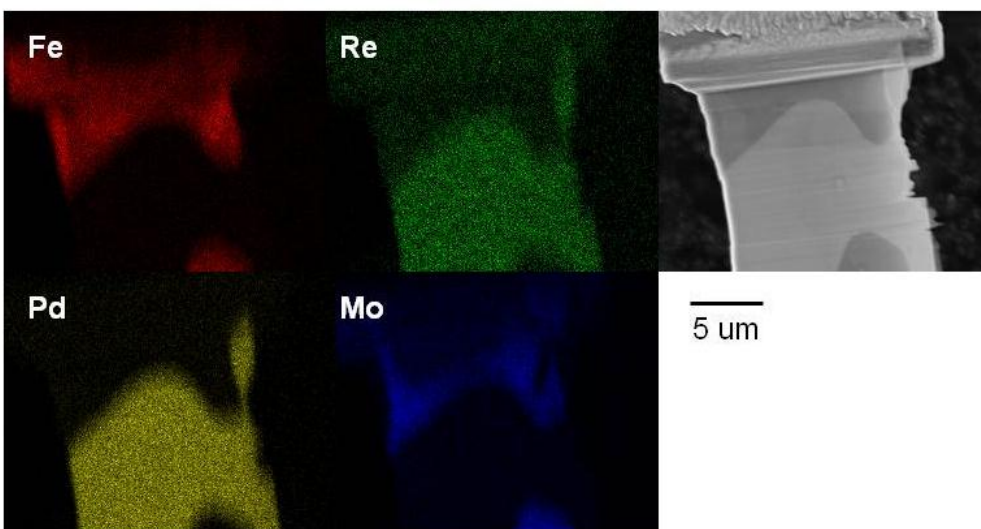


Figure 4.3 Elemental Map showing the occurrence of Re and Pd in the same phase and a significantly lower level of Re in the Mo-Fe intermetallic.

The elemental map in Figure 4.3, shows the regions rich in Pd and Re but that some Re is present in the Fe<sub>2</sub>Mo phase. Evidence from the literature suggests that the formation of the intermetallic is dependent on the presence of some other minor elements [14]. The grayscale image shows the FIB sample. The top portion is the attachment to the grid. On the right hand side, the ion milled region can be seen. The ion milling was not completely successful, following the initial successful extraction of a region of interest, as the material tended to ‘melt’ instead of thin.

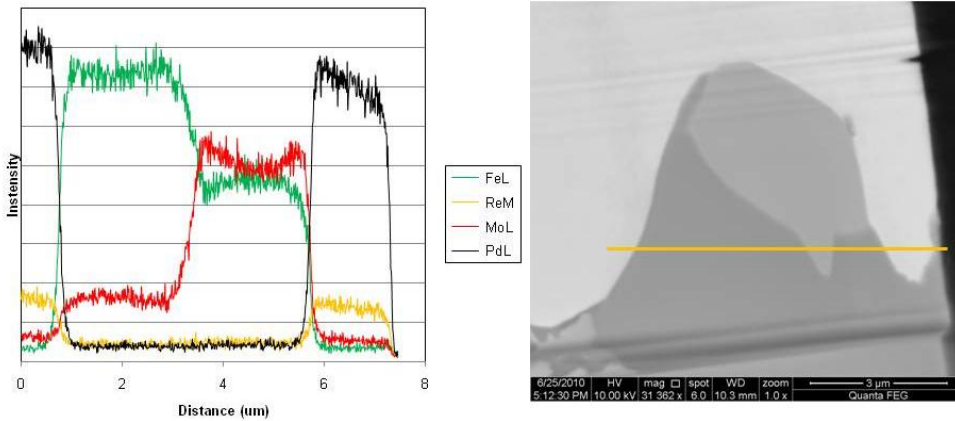


Figure 4.4 Line profiles through different phases in the UDS alloy

In Figure 4.4 and Figure 4.5, the line profile shows the composition of the different phases across several boundaries.

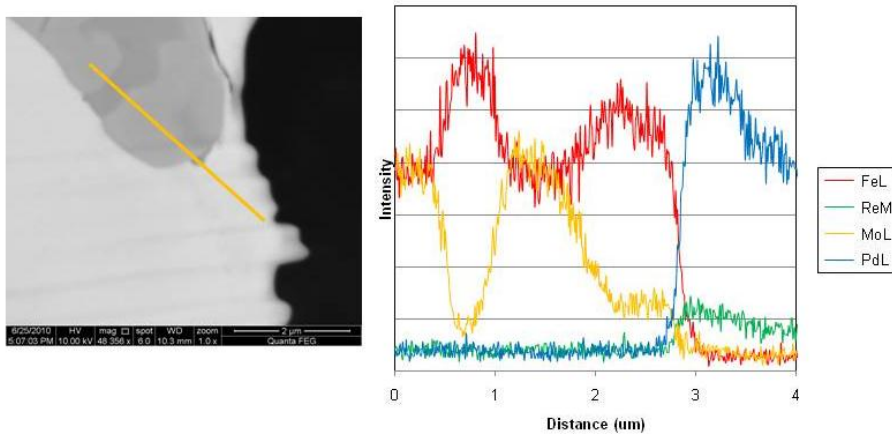


Figure 4.5 Plot showing the distribution of elements across the Pd-rich and intermetallic regions

The line plots reflect the distribution of elements across the boundaries of the major phases in the UDS alloy sample. The plots reflect the three major phases; Fe, Fe<sub>2</sub>Mo, and the Pd-Re-rich alloy. The introduction of Pd as UDS material into the Fe-Mo alloy composition, has reduced the concentration of Re to non-detectable levels in the intermetallic phase and led to a three-phase system in the alloy. It might be expected that Tc will also partition to the UDS rich components. The sample was analyzed in the TEM but proved to be too thick for useful analyses.

## 5. Discussion

The Fe-Mo phase diagram exhibits two peritectic reactions;  $\text{Mo} + \text{L} \rightarrow \sigma (\text{Fe}_{47}\text{Mo}_{53})$  and  $\sigma + \text{L} \rightarrow \text{Fe}_{63}\text{Mo}_{37}$  at 1611°C and 1488°C, respectively (see Figure 1). The R-phase with a composition around  $\text{Fe}_3\text{Mo}_2$  occurs between 1200°C and 1488°C [12]. Doi et al. [13] used TEM to investigate the R-phase through arc-melting followed by quenching and then heat treatment at 1250°C to simulate the  $\text{bcc} \rightarrow \text{bcc} + \text{R}$  reaction. The hexagonal C14-phase  $\text{Fe}_2\text{Mo}$ , forms through a peritectoid transformation at 950°C [14]. Equilibrium between  $\alpha$ -Fe (bcc) and the  $\text{Fe}_2\text{Mo}$  Laves phase is expected at 500°C [11]; whereas at higher temperatures, equilibrium with the  $\mu$ - or R- phase may occur. The Laves phase is stable within a small composition range below 500°C. It has been assumed that the  $\text{Fe}_2\text{Mo}$  phase is not a binary one but requires stabilization through impurities. Hence, the occurrence of Re and Tc may help in the stabilization of this phase as well as nuclear waste forms are prone to contain impurities. It is reasonable that Tc and Re substitute on the A site. These Fe-based Laves phases with the formula  $\text{Fe}_2\text{M}$  (where M can be a transition metal) possess a close packed structure and are a detrimental phase in ferritic steels but are used as strengtheners for austenitic heat-resistant steels that are run under high temperature steam conditions. Mo has a higher solid solution strengthening effect and lower diffusivity in  $\alpha$ -Fe than other elements such as niobium. When compared to the results from Ishikawa et al. [15], the composition of the intermetallic phases in FeMo-Re and FeMo-Tc alloy samples in this study were similar. Ishikawa et al. [15] showed XRD evidence for the presence of the C14 intermetallic phase ( $\lambda$ ). Hence, the result in this study is also consistent with the findings reported in [15]. The importance of C14 Laves intermetallics in metallic waste forms for the incorporation of fission products and actinides has been noted in this study and in others [2,16,17]. Although compositionally different from the phases discussed in [2], we have shown that the C14 Laves intermetallics are responsible for the incorporation of Tc within this Fe-Mo compositional range. However, with the presence of UDS stimulant elements (Pd and Rh), Re appears to be incorporated into these phases. The Pd-Rh phases are hexagonal close packed structures structurally similar to the 5-metal particles found in UO<sub>2</sub> spent nuclear fuels.

In this study, we show that the behavior of Tc and Re in metallic alloys is also similar and that useful predictive assessments of Tc melt behavior may be possible by studying the non-radioactive Re system. In the UDS sample, the introduction of Pd and Rh, resulted in the

formation of phases that dissolved Re. Based on the similar behavior of Tc and Re, this result suggests that the a Tc-bearing UDS sample would behave similarly and the Fe<sub>2</sub>Mo intermetallic would not contain any Tc in this composition.

## 6. Conclusion

Identification of the intermetallic phase with XRD and TEM led to different conclusions. The XRD suggested an orthorhombic phase; however, the occurrence of multiple phases in the same spectra may have led to this result. The TEM data on the dominant Fe-Mo phase, seems to indicate a Fe to Mo ratio of approximately 2 to 1. The concentration of Tc and Re in the FeMo-Tc and FeMo-Re alloy appears to be between 2 and 11 atomic% for both phases. This is a significant quantity that may have led to structural changes over a pure Fe-Mo phase. The intermetallic phases observed in the FeMo alloys were structurally and compositionally similar. This would indicate that Re is a good substitute for Tc in these metallic phases. The electron diffraction patterns suggested a Laves-type C14 phase. This identification is consistent with literature studies on the Fe-Mo system and the conditions of formation. Many binary Laves phases can dissolve comparably large amounts of a third element without changing their crystallographic structure type. It is possible that these elements (Tc and Re) stabilize the intermetallic phase in the waste form alloy.

## 7. References

- [1] T.A. Todd, R.A. Wigeland, Advanced separation technologies for processing spent nuclear fuel and the potential benefits to a geologic repository. Separations for the Nuclear Fuel Cycle in the 21st Century, 2006. 933: p. 41-55.
- [2] W. Ebert, A Strategy for Conditioning TRUEX Raffinate Waste Form Immobilization. Advanced Fuel Cycle Initiative report, AFCI-SUI-WAST-WAST-MI-DV-2009-000001, 2009.
- [3] D. P. Abraham, N. Dietz, N., "Role of Laves intermetallics in nuclear waste disposal," Mater. Sci. Eng., A329-331 (2002) 610-615.
- [4] D. P. Abraham, J. W. Richardson Jr., S. M. McDeavitt, "Laves intermetallics in stainless steel-zirconium alloys," Mater. Sci. Eng., A239 (1997) 658-664.
- [5] D. P. Abraham, J. W. Richardson Jr., S. M. McDeavitt, "Microscopy and Neutron Diffraction Study of a Zirconium-8wt% Stainless Steel Alloy." J. Mater. Sci. 36 (2001) 5143-5154.
- [6] D. S. Gelles, R. M. Ermi, E. C. Buck, R. J. Seffens, C. E. Chamberlin, Technetium Waste Form Development- Progress Report. Pacific Northwest National Laboratory report PNNL-18055, 2009.
- [7] S. Frank, T. O'Holleran, T., P. Hahn, Composition of Tc-Fe Alloy Produced for Testing, Fuel Cycle Research & Development report, FCRD-WAST-000011, 2009.
- [8] F. Poineau, T. Hartmann, P. F. Weck, E. Kim, S. Chinthaka, G. D. Jarvinen, K. R. Czerwinski, "Structural studies of technetium-zirconium alloys by x-ray diffraction, high resolution electron microscopy, and first-principles calculations," Inorg. Chem. 49 (2010) 1433-1438.
- [9] M. Zinkevich, N. Mattern, N., "Thermodynamic modeling of the Fe-Mo-Zr system," Acta Materialia, 50 (200) 3373-3383.
- [10] D. R. G. Mitchell, "DiffTools: Electron diffraction tools for DigitalMicrograph," Micro. Res. Techniq. 71 (2008) 588-593.
- [11] D. Isheim, "Metastable phase formation during the decomposition of Fe-20at% Mo," Acta Mater. 48 (2000) 2873-2883.
- [12] C. P. Heijwegen, G. D. Rieck, "Determination of the Phase Diagram of the Mo-Fe system using diffusion couples," J. Less Common Metals. 37 (1974) 115-121.
- [13] T. Doi, M. Tanimura, Y. Koyama, "Crystal-structure units of the *R* (Fe<sub>3</sub>Mo<sub>2</sub>) phase in the Fe-Mo alloy system," Phys. Rev. B77 (2008) 134205-1.

- [14] Stein F, Palm M, Sauthoff G. 2005. “Structure and stability of Laves phases part II— structure type variations in binary and ternary systems,” *Intermetallics* 13, 1056-1074.
- [15] Ishikawa, S., Matsuo, T., Takeyama, M. 2007. “Phase Equilibria Among  $\alpha$ -Fe,  $\gamma$ -Fe and Fe<sub>2</sub>Mo Phases and Stability of the Laves Phase in Fe-Mo-Ni Ternary System at Elevated Temperatures,” *Materials Research Society Symposium Proceedings*. 980.
- [16] Keiser, D. D., Abraham, D. P., Richardson, J. W. 2000. “Influence of technetium on the microstructure of a stainless steel-zirconium alloy,” *Journal of Nuclear Materials*, 277, 333-338.
- [17] McDeavitt, S. M., Abraham, D. P., Park, J. Y. 1998. “Evaluation of stainless steel-zirconium alloys as high-level nuclear waste forms,” *Journal of Nuclear Materials*, 257, 21-34.

## ACKNOWLEDGEMENTS

This work was supported by the US Department of Energy, Office of Nuclear Energy, Fuel Cycle Research & Development Program under Contract. Bruce Arey and Libor Kovarik are thanked for the preparation of the FIB preparation of a non-radioactive specimen. Programmatic guidance provided by T. Todd (INL) and J. Vienna (PNNL) is gratefully acknowledged. Pacific Northwest National Laboratory is operated for the U.S. Department of Energy by Battelle under Contract DE-AC05-76RL01830.